



# HYPERBOLIC PLYKIN ATTRACTOR CAN EXIST IN NEURON MODELS

VLADIMIR BELYKH

*Mathematics Department, Volga State Academy,  
5, Nesterov st., Nizhny Novgorod 603 600, Russia*

IGOR BELYKH\*

*Laboratory of Nonlinear Systems,  
Swiss Federal Institute of Technology Lausanne (EPFL),  
EPFL-IC-ISC-LANOS, Station 14, 1015 Lausanne, Switzerland  
igor.belykh@epfl.ch*

ERIK MOSEKILDE

*Department of Physics, The Technical University of Denmark,  
2800 Kongens Lyngby, Denmark*

Received December 30, 2004; Revised January 30, 2005

Strange hyperbolic attractors are hard to find in real physical systems. This paper provides the first example of a realistic system, a canonical three-dimensional (3D) model of bursting neurons, that is likely to have a strange hyperbolic attractor. Using a geometrical approach to the study of the neuron model, we derive a flow-defined Poincaré map giving an accurate account of the system's dynamics. In a parameter region where the neuron system undergoes bifurcations causing transitions between tonic spiking and bursting, this two-dimensional map becomes a map of a disk with several periodic holes. A particular case is the map of a disk with three holes, matching the Plykin example of a planar hyperbolic attractor. The corresponding attractor of the 3D neuron model appears to be hyperbolic (this property is not verified in the present paper) and arises as a result of a two-loop (secondary) homoclinic bifurcation of a saddle. This type of bifurcation, and the complex behavior it can produce, have not been previously examined.

*Keywords:* Plykin attractor; neuron model; geometrical approach.

## 1. Introduction

Dissipative dynamical systems with a unique saddle-type equilibrium point play a significant role in bifurcation theory [Shilnikov *et al.*, 1998, 2001] and often exhibit dynamical chaos associated with funnel-like attractors. Such attractors can arise, for example, in 3D systems where the unstable two-dimensional (2D) manifold of the saddle-type equilibrium returns into the equilibrium's

neighborhood along a one-dimensional (1D) stable manifold. This leads to the formation of a funnel-like trapping zone for the trajectories coming from the outside. This construction was introduced by Shilnikov [1984] for the saddle-focus case, and spiral chaos inside the funnel was subsequently studied by Ovsyannikov and Shilnikov [1992]. In the present paper, we consider the case where a 3D system has a unique *saddle* equilibrium point, and

---

\*Author for correspondence. Permanent address: Department of Mathematics and Statistics, Georgia State University, 30 Pryor Street, Atlanta, GA 30303, USA. E-mail: ibelykh@mathstat.gsu.edu

study bifurcation sets and the emergence of strange attractors.

As a first example of systems with the funnel-like structure of the trapping zone, we consider a slow-fast model of bursting neurons. Bursting occurs when neuron activity alternates, on a slow time scale, between a quiescent state and fast repetitive spiking. Over the years, much work has been devoted to the classification of various types of bursting [Rinzel, 1987; Rinzel & Ermentrout, 1989; Izhikevich, 2000; Golubitsky *et al.*, 2001]. Chaos in neuron models and routes describing possible transitions between tonic spiking and bursting were extensively studied in a series of papers [Terman, 1991, 1992; Wang, 1993; Belykh *et al.*, 2000; Guckenheimer & Oliva, 2002; Shilnikov *et al.*, 2005; Shilnikov & Cymbalyuk, 2005]. In particular, it was shown [Belykh *et al.*, 2000; Shilnikov *et al.*, 2005] that a homoclinic bifurcation of a saddle-node periodic orbit leads to the spiking-bursting transition. Neuron models can demonstrate surprising bifurcation phenomena: The first example of the emergence of the blue-sky catastrophe [Palis & Pugh, 1974; Turaev & Shilnikov, 1995] in real physical systems was discovered in a biologically relevant neuron model [Shilnikov & Cymbalyuk, 2005].

Models of bursting neurons continue to surprise us: In this paper, we show how a generic neuron model undergoes new, unstudied homoclinic bifurcations and that it can display the *hyperbolic Plykin attractor* [Plykin, 1974]. In fact, while examples of structurally stable (hyperbolic) strange attractors for two- and three-dimensional diffeomorphisms have been known for some time (see an extensive review in [Guckenheimer & Holmes, 1990]), hyperbolic attractors in flows corresponding to real physical systems have not previously been observed. The Lorenz attractor contains only unstable trajectories and, loosely speaking, has the property of hyperbolicity, but this attractor is structurally unstable (it does not persist under perturbations) and only considered as quasi-hyperbolic. To the best of our knowledge, there is only one example of a system of differential equations admitting a strange hyperbolic attractor. This example is due to Hunt and Mac Kay [2003].

Using a geometrical approach to the study of the global dynamics in a neuron model with a single equilibrium and constructing the Poincaré return map, we show that all the topological prerequisites for the existence of a hyperbolic attractor are met, and that the system has an attractor homotopic to

the Plykin one. This funnel-like attractor, defined by the Poincaré map with three holes, occurs as a result of a two-loop (secondary) homoclinic bifurcation of the saddle and shows the possibility for the existence of a hyperbolic attractor in a realistic neuron model. The question whether the discovered attractor is hyperbolic in a strict mathematical sense, requires a separate careful study and remains open.

Subsequent bifurcations of multiloop homoclinic loops can lead to the emergence of even more complicated attractors defined by mappings with  $k$  ( $k > 3$ ) holes. It is worth noticing that these Plykin-like attractors occur in a parameter region where the neuron system undergoes bifurcations causing transitions between tonic spiking and bursting. Such attractors and bifurcations leading to their emergence have not been studied yet within the framework of the bifurcation theory. Consequently, the classification of all possible routes of transitions between tonic spiking and bursting seems to be *unrealistic* and the details of this transition remain a fundamental problem for the theory of dynamical systems.

Our analysis proceeds along the following scheme: The basic model and the corresponding assumptions are presented in Sec. 2. We consider a conductance-based neuron model in the form of a 3D system of differential equations with two fast and one slow variable. Section 3 presents the construction of the global cross-section and a geometrical analysis of the flow-defined Poincaré map. We show that depending on the bifurcation parameter, this mapping is (i) a map of a disk into itself; (ii) a map of the disk into an annulus; (iii) a map of the disk with several periodic holes. In the latter case, where complicated spiking-bursting transitions are possible, there exists a family of Plykin-like attractors. Based on these results, in Sec. 4, we present an argument for the existence of a Plykin attractor and discuss a series of new loop-adding homoclinic bifurcations leading to its emergence and disappearance. We show that the destruction of the simplest one-loop homoclinic loop can already lead to the emergence of a complex limit set associated with a Smale horseshoe.

## 2. The Model

Models of bursting neurons can often be represented by the following singular perturbed system (see, e.g.

[Hindmarsh & Rose, 1984; Rinzel, 1987])

$$\dot{x} = X(x, z), \quad \dot{z} = \mu(Z(x) - z - \delta), \quad (1)$$

where  $x = (x_1, x_2)$  corresponds to two fast variables and represents the membrane potential and a fast current, respectively. The scalar variable  $z$  is associated with a slow current. The functions  $Z : R^2 \rightarrow R^1$  and  $X : R^2 \rightarrow R^2$  are assumed to be smooth enough. The function  $Z(0) = 0$ , the parameter  $\mu$  is small and  $\delta$  is a bifurcation parameter.

For  $\mu = 0$ , the fast reduced subsystem

$$\dot{x} = X(x, z), \quad z = \text{const} \quad (2)$$

defines a  $z$ -parameter family of two-dimensional phase portraits. This represents the usual adiabatic approach in which the reduced system ( $\mu = 0$ ) accounts for the fast dynamics, and variations of  $z$  describe the slow dynamics for  $\mu > 0$ .

The functions  $X(x, z)$  and  $Z(x)$  satisfy the following typical assumptions.

- (i) The fast subsystem (2) has three branches of equilibrium points  $\{X(x, z) = 0\}$ :  $b_0^l = \{x = x_l(z)\}$ ,  $b_0^m = \{x = x_m(z)\}$  and  $b_0^r = \{x = x_r(z)\}$  (see Fig. 1). In the region of interest, the right branch corresponds to a family of

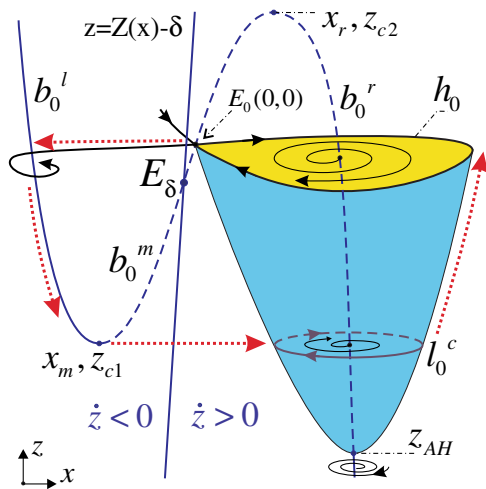


Fig. 1. Assumed arrangement of the trajectories in the neuron model. The family of phase portraits of the fast system is shown as a  $z$ -parameter bifurcation diagram. The blue  $z$ -shaped curve represents the equilibria of the fast system and consists of three branches:  $b_0^l$ ,  $b_0^m$  and  $b_0^r$ . The cyclic (parabolic) surface is composed of stable limit cycles  $l_0^c$  of the fast system. The intersection between the surface  $\kappa$  and  $b_0^m$  defines the coordinates of the full system saddle equilibrium  $E_\delta$ . The red dotted curve schematically illustrates the route for bursting that exists in the slow-fast system.

unstable equilibria of system (2) and meets the middle branch at the point  $z_{c2} > 0$ :  $x_m(z_{c2}) = x_r(z_{c2})$ . The middle and the left branches merge at the point  $z_{c1} < 0$ ,  $x_l(z_{c1}) = x_m(z_{c1})$ , corresponding to a saddle-node equilibrium. The middle branch, defined for  $z \in (z_{c1}, z_{c2})$ , passes zero,  $x_m(0) = 0$ , and consists of a family of saddles. The left branch is a curve of stable equilibria. Without loss of generality, we may assume that the left branch is composed from stable foci with a counter-clockwise rotation direction. This is consistent, for example, with the arrangement of trajectories in the Hindmarsh–Rose model [Hindmarsh & Rose, 1984].

- (ii) For  $z < 0$ , the fast subsystem (2) has a stable limit cycle  $l_0^c = \{x = x_0(t, z)\}$  of the period  $\tau(z) = 2\pi/\omega(z)$ . The cycle  $l_0^c$  encloses the unstable equilibrium branch  $b_0^r$  and constitutes a cyclic surface for  $z \in (z_1, 0)$ ,  $z_1 < 0$ . For definiteness, we assume that the cycle  $l_0^c$  is born through a supercritical Andronov–Hopf bifurcation at  $z = z_{AH}$ . However, our analysis is directly applicable to any other reduced system family of limit cycles, displaying a homoclinic bifurcation to the saddle  $E_0$ . This results in the following assumption.
- (iii) For  $z = 0$ , the saddle point  $E_0(x_m = 0, z = 0)$  of the fast subsystem (2) has a homoclinic orbit  $h_0 = \{x = x_0(t, 0)\}$ , which is the topological limit of the stable limit cycle. This cycle merges with the manifolds of  $E_0$  as the parameter  $z$  approaches zero from below. The corresponding saddle value of  $E_0$  is negative:  $\sigma_0 = \lambda_1^0 + \lambda_2^0 < 0$ , where  $\lambda_1^0 < 0 < \lambda_2^0$  are the eigenvalues of the fast system's saddle.
- (iv) The arrangement of the family of saddle separatrices for the fast system is assumed to be as illustrated in Figs. 1 and 2. The stable and unstable separatrices constitute the surfaces  $W_0^s$  and  $W_0^u$ , respectively (see Fig. 2).

To proceed with the study of the dynamics of the full system, we must first construct a global cross-section  $D_0$  of the fast system, by connecting the left and right branches of equilibria,  $b_0^l$  and  $b_0^r$ , as shown in Fig. 2. The unstable and stable manifolds,  $W_0^u$  and  $W_0^s$ , transversally intersect the global cross-section  $D_0$  by the green and blue lines  $w_0^{u1}$ ,  $w_0^{u2}$ , and by the violet line  $w_0^s$ , respectively (see Fig. 2).

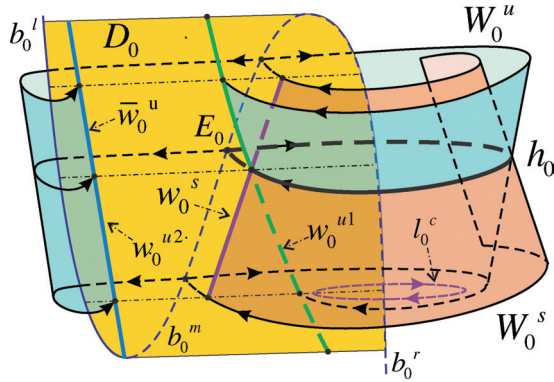
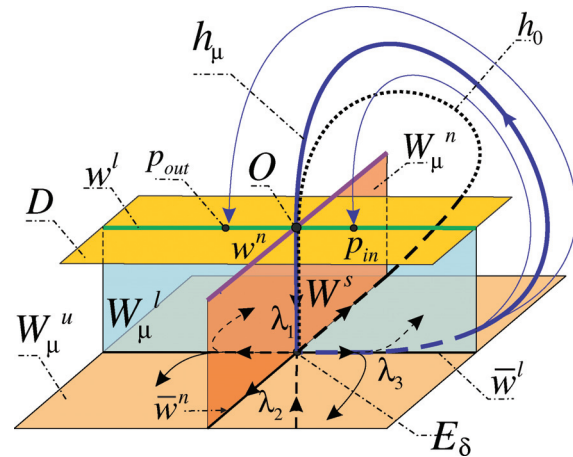


Fig. 2. Unstable and stable manifolds of the saddle  $E_0$  intersect the cross-section  $D_0$  of the fast system by the green and blue lines  $w_0^{u1}$ ,  $w_0^{u2}$ , and by the violet line  $w_0^s$ , respectively. The homoclinic orbit  $h_0$  is formed by the transversal intersection between  $W_0^s$  and  $W_0^u$ .

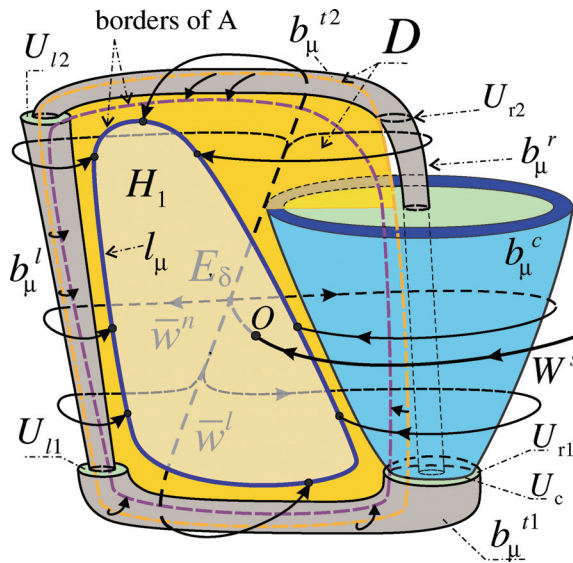
(v) This assumption is related to the full system (1). The surface  $\kappa = \{z = Z(x) - \delta\}$  intersects the middle branch of equilibria and separates the phase space of system (1) into two domains:  $Ph^+$ , where  $\dot{z} > 0$  and the variable  $z(t)$  increases with time, and  $Ph^-$ , where  $\dot{z} < 0$  and  $z(t)$  is decreasing along the trajectories of system (1). Let the slow-fast system (1) have a *unique* equilibrium point  $E_\delta$ . Therefore, we assume that the scalar product of the vector tangent to  $b_0^m$  and of the gradient of  $(Z(x) - z - \delta)$  is positive at  $E_\delta$ , i.e.  $\lambda^0 = (Z_x x'_m - 1)|_{E_\delta} > 0$ . This implies that the middle branch  $b_0^m$  of saddles transversally enters into the region  $Ph^+$  when  $z$  increases. For convenience, we assume that the  $z$ -coordinate of the saddle  $E_\delta$  satisfies the conditions:  $z_0(0) = 0$  and  $z'_0(\delta) > 0$ .

As illustrated in Fig. 3(a), the equilibrium  $E_\delta$  has three real eigenvalues:  $\lambda_1$ ,  $\lambda_2$  and  $\lambda_3$ . Two of them,  $\lambda_1 < 0 < \lambda_2$ , are induced by the fast system's saddle,  $\lambda_{1,2} = \lambda_{1,2}^0 + O(\mu)$ . The third eigenvalue  $\lambda_3 = \lambda^0 \mu + O(\mu^2)$  is positive due to (V). The pair  $(\lambda_2, \lambda_3)$  corresponds to the unstable manifold  $W_\mu^u$ , the pair  $(\lambda_1, \lambda_3)$  defines the leading manifold  $W_\mu^l$ , and the pair  $(\lambda_1, \lambda_2)$  is related to the nonleading manifold  $W_\mu^n$ . The single eigenvalue  $\lambda_1$  determines a 1D stable manifold  $W_\mu^s$ . All these manifolds will approach the corresponding manifolds of the fast system while the parameter  $\mu$  decreases.

The dynamics of the full system essentially depends on the position of the separating surface  $\kappa = \{z = Z(x) - \delta\}$  and the small parameter  $\mu$ .



(a)



(b)

Fig. 3. (a) The leading and nonleading manifolds,  $W_\mu^l$  and  $W_\mu^n$ , of the full system's saddle  $E_\delta$  intersect the global cross-section  $D$  by the green and violet lines,  $w^l$  and  $w^n$ , respectively. (b) Construction of the Poincaré map. See the text for a detailed explanation.

It is well known [Terman, 1991; Belykh et al., 2000; Shilnikov et al., 2005a] that there exist several important regions of the bifurcation parameter  $\delta = \delta_j(\mu)$ ,  $j = b, h_1, s : \delta_b(\mu) < \delta_{h_1}(\mu) < \delta_s(\mu)$  such that the following properties hold:

- (1) For  $\delta < \delta_b(\mu)$ , the full system (1) has only bursting oscillations. In this case, the surface  $\kappa$  intersects the middle branch of equilibria  $b_0^m$  such as shown in Fig. 1. The cyclic manifold of

the full system (called below the cyclic bundle  $b_\mu^c$ ) is transient for the trajectories, and the bursting oscillation follows the route shown by the red dotted curve in Fig. 1.

- (2) For  $\delta > \delta_s(\mu)$ , the full system (1) has only tonic spiking defined by a stable fast limit cycle. Here, the full system saddle  $E_\delta$  lies on an upper part of  $b_0^m$ , close to the critical point  $(x_r, z_{c2})$ , such that the limit cycle is far from bifurcations.
- (3) For  $\delta_b(\mu) < \delta(\mu) < \delta_s(\mu)$ , both spiking and bursting solutions are possible, and variations of  $\delta$  can cause transitions between them. The bifurcation playing a crucial role in such transitions is a homoclinic bifurcation to the full system saddle  $E_\delta$ . The corresponding homoclinic orbit  $h_\mu = W_\mu^u \cap W_\mu^s$  [see Fig. 3(a)] exists for  $\delta = \delta_{h_1}(\mu)$ . It is worth noticing that in contrast to the homoclinic  $h_0$  of the fast system [also depicted in Fig. 3(a)], giving rise to a stable cycle ( $\sigma_0 < 0$ ), the homoclinic  $h_\mu$  gives birth to a saddle limit cycle (the saddle value  $\sigma = \lambda_1 + \lambda_3 < 0$  and  $\lambda_2 > 0$ ), with an increase of the parameter  $\delta$  from  $\delta_{h_1}$ .

Our main objective is to construct a flow-defined 2D map describing the dynamics on the attractors existing in the three above mentioned regions of parameters and the corresponding bifurcation transitions.

### 3. Poincaré Return Map

We start our study of the system's limit sets by choosing a cross-section  $D$  to the trajectories of the full system (1). This cross-section must be global, i.e. the vector field must be transversal to  $D$  and any trajectory starting from  $D$  must return to this cross-section.

#### 3.1. Global section construction

Denote  $z_1 = z_{c1} + \epsilon_1(\mu)$ ,  $z_2 = z_{c2} - \epsilon_2(\mu)$ , where  $\epsilon_{1,2} \rightarrow 0$  for  $\mu \rightarrow 0$ , and introduce four neighborhoods  $U_{k_i} = \{\|x_k(z_i) - x\| < \epsilon_{k_i}(\mu)\}$ ,  $k = (l, r)$ ,  $i = 1, 2$ . As shown in Fig. 3(b), the disk  $U_{r_2}$  generates an unstable bundle  $b_\mu^r$  by the flow in reverse time, and the disk  $U_{l_2}$  generates a stable bundle  $b_\mu^l$  in direct time. This invariant bundle contains a set of trajectories that are all equivalent and converge to the line of equilibria  $b_0^l$ , for  $\mu \rightarrow 0$ . Introduce a vicinity of the fast system limit cycle  $l_c(z_1)$ ,

$U_c = \{\|x_0(t, z_1) - x\| < \epsilon_c(\mu)\}$ . Consequently, the flow generates a cyclic bundle  $b_\mu^c$ , starting from  $U_c$ . This bundle is continued up to the surface  $\{z = \epsilon'_c(\mu) < 0\}$ , where  $\epsilon_c(\mu)$  and  $\epsilon'_c(\mu)$  vanish for  $\mu = 0$ .

To construct the global section of the full system, close to the fast system global section  $D_0$ , we connect the left and right bundles  $b_\mu^l$  and  $b_\mu^r$  by the following procedure. Starting from  $U_{r_2}$ , we continue the bundle  $b_\mu^r$  by the flow until it terminates in the neighborhood  $U_{l_2}$ , generating the left bundle. The size of  $U_{l_2}$  is being chosen to match the transient bundle  $b_\mu^{t2}$  [see Fig. 3(b)].

Trying to directly complete the loop of the bundle neighborhoods related to the global cross-section, one encounters the following problem: The set of trajectories, coming from the basin of attraction located below the cycle  $l_c(z_1)$  and entering into the cyclic bundle interior  $b_\mu^c$ , is encompassed by the left bundle flow prolongation to the right branch. Therefore, the corresponding low edge of the cross-section  $D$ , that would be mapped back by the flow into  $D$ , is difficult to imagine. To resolve this problem, we formally perform a "surgical attack" on this part of the basin. Namely, instead of this part of the low basin we introduce a new flow mapping  $U_{l_1}$  onto  $U_{r_2}$  and form the transient bundle  $b_\mu^{t1}$ . This completes the loop and does not affect attractors of the full system.

We can now introduce the global section  $D$  as follows: The section  $D$  is  $\mu$ -close to the fast system cross-section  $D_0$ . Its right edge is shifted to the left from the bundle  $b_\mu^r$  [cf. Fig. 3(b)]. This is a necessary condition for this edge to be mapped onto  $D$ . The left edge of  $D$  is chosen arbitrarily inside the left bundle  $b_\mu^l$ . Two remaining parts of the boundary of  $D$  are assumed to connect the left and right edges of  $D$  as shown in Fig. 3(b). The two lines are assumed to be mapped by the flow into  $D$ . Under these assumptions,  $D$  is the global cross-section that allows us to simplify the study of bursting dynamics in the singular perturbed system (1) by considering the Poincaré map  $f$  of  $D$  into itself. The limit sets and bifurcations of the map  $f$  correspond to spiking and bursting attractors, and to transitions between bursting and spiking.

Denote by  $O$ , the point of intersection between the 1D stable manifold  $W_\mu^s$  of the saddle  $E_\delta$  and the global cross-section  $D$ ; and the intersection lines  $w^l = W_\mu^l \cap D$ ,  $w^r = W_\mu^r \cap D$  [cf. Fig. 3(a)]. The map  $f$  has a singularity at the point  $O$ , such that a flow-defined image of the point  $O$  is the equilibrium

point  $E_\delta$ . To eliminate this singularity, we apply the standard method of extension by continuity [Shilnikov *et al.*, 1998]. In this way, the image  $fO$ , depicted by the blue closed curve  $l_\mu$  in Fig. 3(b), is generated by all trajectories of the unstable manifold  $W^u$ , intersecting the cross-section  $D$ . Consequently, the topological disk  $D$  is mapped by the map  $f$  into itself, such that the image  $fD$  is an annulus  $A$  with the hole  $H_1$ . The annulus is bounded by the following curves: The inner line is  $l_\mu$ , the border of the hole  $H_1$ , and the outer curve is the

image  $fD$  of the cross-section edge [the violet dashed line in Fig. 3(b)]. The part of the 2D unstable manifold  $W_\mu^u$ , connecting the saddle  $E_\delta$  to the hole boundary  $l_\mu$ , together with the hole  $H_1$  forms a heart shape trapping zone  $G$  for the trajectories of system (1). All trajectories starting from  $G$  will stay there forever. Trajectories from the outside enter into  $G$  through the hole  $H_1$  [see Fig. 4(a)]. Consequently, the map  $f$  is a global Poincaré return map and represents the complete set of attractors and bifurcations of system (1).

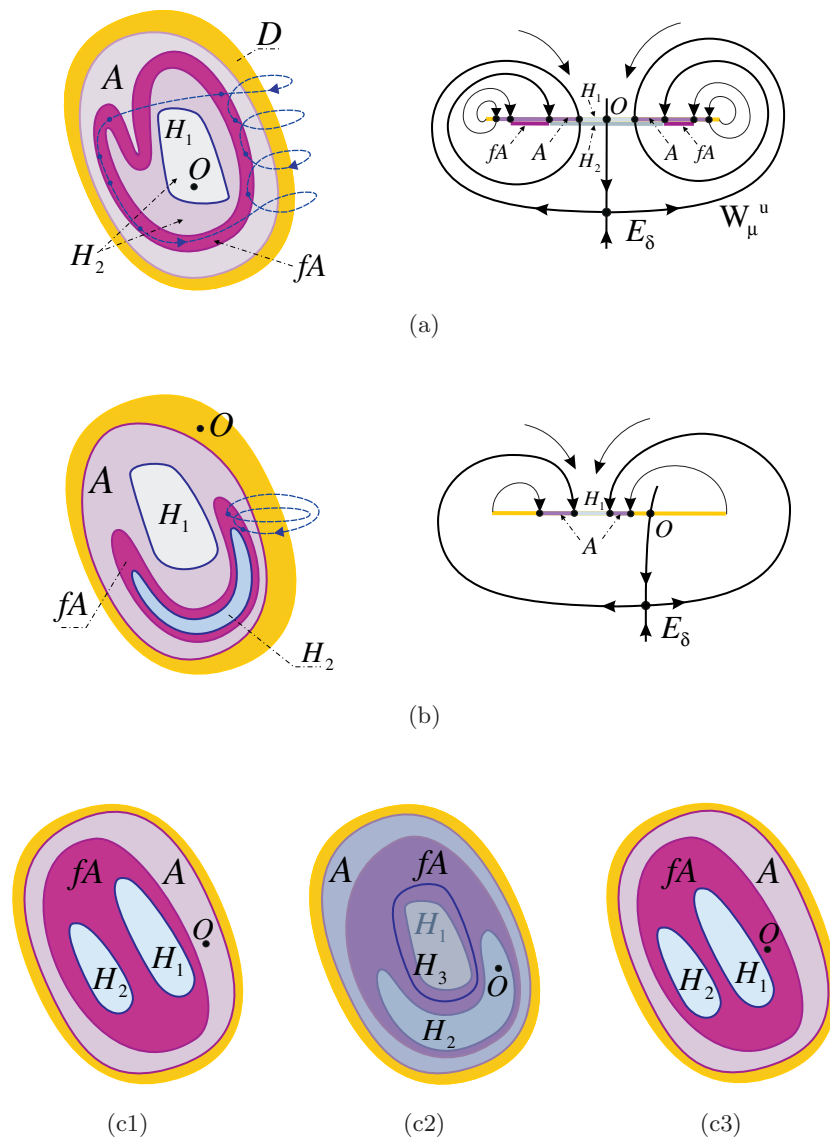


Fig. 4. Schematic pictures illustrating possible positions of the point  $O$  with respect to the annulus  $A$  and the hole  $H_1$ . (a) Case 1:  $\delta < \delta_{h_1}$ . Bursting is depicted by the blue dashed line (left). Schematic sketch for the system's projection onto a plane perpendicular to the disk  $D$ . The 2D unstable manifold  $W_\mu^u$  forms a funnel-type trapping zone  $G$ . Trajectories from the outside enter into  $G$  through the hole  $H_1$  (right). (b) Case 2:  $\delta > \delta_s$ . (c1)–(c3) Case 3:  $\delta_{h_1} < \delta < \delta_s$ : (c2) The formation of a map with two periodic holes  $H_1$  and  $H_2$ .

### 3.2. Limit sets of the map $f$

Let  $u \in R^2$  be the vector coordinate in  $D$ , then the one-to-one map  $f$  of the disk  $D$  into the annulus  $A$  reads:  $u(i + 1) = f(u(i))$ ,  $i \in Z$ . The map  $f$  has a closed invariant limit set of discrete trajectories  $\Omega$ , such that all the attractors of  $f$  lie in  $\Omega$ . Let  $u = u^a(i)$  be an attracting trajectory of  $f$ .

It follows from the map construction that if two subsequent iterates of  $f$ ,  $u^a(i_1)$  and  $u^a(i_1 + 1)$ , lie in a neighborhood of the cyclic bundle  $b_\mu^c$  then the trajectory of the slow-fast system (1), connecting these points, makes a turn around the bundle  $b_\mu^c$ , corresponding to *one spike*, as shown in Fig. 4(a). If  $u^a(i_1)$  and  $u^a(i_1 + 1)$  fall in a neighborhood of the left bundle  $b_\mu^l$ , then the corresponding trajectory of system (1) slowly drifts down along  $b_\mu^l$  and corresponds to a *quiescent* part of the bursting trajectory. If  $u^a(i_1)$  lies near the bundle  $b_\mu^l$  ( $b_\mu^c$ ), and the next iterate  $u^a(i_1 + 1)$  jumps to a neighborhood of the bundle  $b_\mu^c$  ( $b_\mu^l$ , respectively), then the trajectory connecting the two points corresponds to the *transition* from the quiescent mode to fast repetitive spiking, and vice versa.

Therefore, *bursting* is defined by the attracting trajectories of the map  $f$  visiting both the neighborhoods of  $b_\mu^l$  and  $b_\mu^c$ . Naturally, the trajectories remaining in the neighborhood of the cyclic bundle  $b_\mu^c$ , correspond to *tonic spiking*.

In terms of the map  $f$ , the existence of bursting and spiking-type attractors of system (1) and the transitions between them, essentially depend on the position of the point  $O$  with respect to the annulus  $A$  and the hole  $H_1$ . This position depends on the bifurcation parameter  $\delta$ . Consider separately three nondegenerate cases of the mutual positions between  $O$  and  $A$ , related to the following regions of the bifurcation parameter  $\delta$ : (1)  $\delta < \delta_{h_1}(\mu)$ ; (2)  $\delta > \delta_s(\mu)$ ; (3)  $\delta_{h_1}(\mu) < \delta < \delta_s(\mu)$ , where  $\delta_{h_1}(\mu)$  and  $\delta_s(\mu)$  are the above mentioned values of the parameter  $\delta$ . Note that if the point  $O$  lies on the border of the hole  $H_1$ , then system (1) undergoes a homoclinic bifurcation for  $\delta = \delta_{h_1}(\mu)$ , providing the transition from cases 1 to 3 with an increase in  $\delta$ .

#### 3.2.1. Case 1: $\delta < \delta_{h_1}(\mu)$

The point  $O$  lies inside the hole  $H_1$  [see Fig. 4(a)]. In terms of system (1), this situation corresponds to the existence of bursting-type attractors in the subregion  $\delta < \delta_b < \delta_{h_1}$  and to possible spiking-bursting transitions in the subregion  $\delta_b < \delta < \delta_{h_1}$ .

When the point  $O$  lies inside the hole  $H_1$ , the map  $f$  is a smooth diffeomorphism of the annulus  $A$  into itself, such that  $H_1 \subset fH_1 = H_2$ ,  $fA \subset A$ , and  $H_2$  is the hole of the annulus  $fA$ . Further iterates of the map  $f$  give the embedding:  $H_1 \subset H_2 \subset \dots \subset H_k = f^{k-1}H_1$ ,  $f^kA \subset f^{k-1}A$ . In other words, the size of the holes increases from iteration to iteration, and the width of the iterated annulus  $f^kA$  decreases and approaches to an attracting set for  $k \rightarrow \infty$ . The theory of such maps is intensively studied by Shilnikov and collaborators (see the comprehensive review in [Shilnikov *et al.*, 2004]). This theory is related to the existence of closed invariant curves  $J \subset A$  with the dynamics of  $f|_J$  defined by the unique Poincaré rotation number, and to the torus breakdown bifurcations. Let us specify the rotation number for the map  $f$ .

**Definition 1.** Let  $u = \xi(\theta, \rho)$  be a map of a lifted ring:  $\{\theta \in R^1, \rho_1 < \rho < \rho_2\}$  onto the annulus  $A$ . Let  $u^*(i)$  be a trajectory from the limit set of  $f$ , such that  $u^*(i) = \xi(\theta^*(i), \rho^*(i))$ . The rotation number is defined as

$$r(u^*) = \overline{\lim}_{i \rightarrow \infty} \frac{\theta^*(i)}{2\pi i}.$$

When system (1) displays a bursting solution (surely, for  $\delta < \delta_b(\mu)$ ), the bursting trajectories rotate along the annulus  $A$ , therefore the rotation number  $r(\Omega) > 0$ . When the point  $O$  is far from the border  $l_\mu$  of the hole  $H_1$ , i.e.  $|\delta|$  is large, the rotation number is often unique, and the slow-fast system (1) is far from bifurcations and exhibits periodic regular bursting. On the other hand, when the difference  $\delta - \delta_{h_1} < 0$  is small ( $O$  is close to the border of  $H_1$ ), the shape of the first annulus image changes as follows.

**Statement 1.** If  $O \in H_1$ , and  $O$  is close to the boundary  $l_\mu$ , then the image of the annulus  $fA \subset A$  has a  $Z$ -shape fold [see Fig. 4(a)]. The closer the point  $O$  approaches  $l_\mu$ , the larger the fold becomes.

*Proof.* The point  $O$  is the intersection of the curves  $w^l = W_\mu^l \cap D$ , and  $w^n = W_\mu^n \cap D$  [see Fig. 3(a)]. In a neighborhood of the saddle  $E_\delta$ , the unstable node on the surface  $W_\mu^u$  generates a foliation of the integral surfaces spanning along the 1D stable manifold  $W_\mu^s$ . The intersection of this foliation and the global cross-section  $D$  has a similar unstable node foliation structure of the lines for which  $w^l$  and  $w^n$  play the role of leading and nonleading directions.

The line  $l_\mu$  is tangent to a curve  $\gamma_c \subset fl$  at the point  $\zeta_c$ . Curves of the foliation, located below this curve, have no intersections with  $l_\mu$ , and each curve of the foliation above this tangent curve has two points of intersection  $\zeta_1, \zeta_2$  with  $l_\mu$ . Therefore, the image  $f(\zeta_c)$  is a critical point of  $f(l_\mu)$ , and the images  $f(\zeta_1)$  and  $f(\zeta_2)$  are the points on the opposite leaves of the fold. The image of the external edge of  $A$  has a similar shape. Consequently, the annulus image has a fold, and Statement 1 holds. ■

Subsequent images  $f^2A, f^3A, \dots, f^kA$  preserving their original  $Z$ -shape are shifted along the annulus, when iterated. Therefore, if we chose a rectangular  $P$  (not depicted in Fig. 4) on the cross-section  $D$  such that  $P$  lies in a vicinity of  $O$  and joins the leading line  $w^l$  by its large part, then the  $k$ -iterate  $f^kP$  can reach and overlap its original preimage  $P$ . This leads to the formation of either a transversal complete Smale horseshoe, first discovered in bursting transitions by Terman [1991, 1992], or of a tangent horseshoe in formation. In either case, complex dynamics arises. More precisely, in the first case, the saddle chaotic component of the limit set  $\Omega$  is always present, and all the trajectories generated by the horseshoe are unstable. In the second case, the control parameter  $\delta$  enters into the Newhouse regions, corresponding to the coexistence of an infinite number of stable bursting attractors with infinitely small basins of attraction [Gavrilo & Shilnikov, 1972; Newhouse, 1974; Gonchenko et al., 1996]. This results in rotation number scattering [Belykh et al., 1977] together with an uncertainty in bursting–bursting transitions. In other words, a tiny change of  $\delta$  leads to jumps from one attracting state of bursting to another with a different rotation number. Moreover, the attracting states can also have the same rotation number. For example, all the stable bursting solutions coexisting in the Newhouse regions have the same rotation number. The realization of a particular bursting attractor depends on the initial conditions.

### 3.2.2. Case 2: $\delta > \delta_s(\mu)$

The point  $O$  lies outside both the hole  $H_1$  and the annulus  $A$ , i.e.  $O \in D \setminus D_1$ ;  $D_1 = A \cup H_1$  [see Fig. 4(b)]. This is possible if  $\delta > \delta_s(\mu)$ : the limit set  $\Omega = \Omega_s$  has only tonic spiking oscillations. In this case, the saddle  $E_\delta$  lies essentially above the cyclic bundle  $b_\mu^c$  such that the point  $O$  is located between

the right upper edge of the disk  $D$  and the edge of the annulus  $A$  [cf. Figs. 3(b) and 4(b)].

In this case, the map  $f$  becomes a diffeomorphism of the disk  $D$ . The hole  $H_1$  is mapped into a sequence of nonoverlapping holes  $H_k = f^{k-1}H_1$ ,  $k = 1, 2, \dots$  indicating an extended area of the basin.  $fD \subset D$  and the map  $f$  has the limiting set  $\Omega_s$ , inclusive of at least one fixed point. The set  $\Omega_s$  is located in the vicinity of the cycle bundle  $b_\mu^c$  and corresponds to a fast limit cycle with zero rotation number  $r(\Omega_s)$ . The map  $f$  has a similar property in the case, where the singularity point  $O$ , staying inside the annulus  $A$ , lies outside the  $k$ -iterate image of  $D$ .

The tonic spiking dynamics in the considered region can also be complicated. As shown in [Terman, 1991; Wang, 1993], there exists a hyperbolic structure (the chaotic saddle) similar in many respects to a Smale horseshoe. The typical transition from simple to complex spiking occurs along the following scheme. The fast one-period cycle undergoes a period-doubling cascade of bifurcations, finally reaching the Newhouse regions and transversal Smale horseshoes with an attracting complement. All the coexisting spiking solutions have the zero rotation number  $r(\Omega) = 0$ . The description of this spiking transition is due to Wang [1993].

### 3.2.3. Case 3: $\delta_{h_1}(\mu) < \delta < \delta_s(\mu)$

The point  $O$  lies inside the annulus  $A$  and is not located in the hole  $H_1$  [see Fig. 4(c)]. This is the most interesting case corresponding to spiking–bursting transitions, where the Plykin-like attractors can occur.

After the first iterate of the map  $f$ , three non-degenerate possibilities arise for the mutual position between  $O$ ,  $fA$ , and  $fH_1 = H_2$ .

- (1)  $O \in A$ , but  $O \notin fD_1$  [Fig. 4(c1)]. The further application of the map  $f$  to the disk  $D_2 = fA \cup H_1 \cup H_2$ , leads to the picture from Case 2. Here,  $f : D_2 \rightarrow D_2$  is a diffeomorphism of a disk with the property that  $fH_1 = H_2$ , and  $f^{k-1}H_1 = H_k$ ,  $k = 1, 2, \dots$  are nonoverlapping disks belonging to the basin of attraction. The main property of this map is that the diffeomorphism  $f$  has at least one fixed point.
- (2)  $O \in H_2$ . The image of  $H_1$ , the hole  $H_2$ , covers the singularity point  $O$  outside the hole  $H_1$  such as shown in Fig. 4(c2). The second image of  $H_1$ ,

the hole  $H_3$ , covers  $H_1$ . The next iterate of  $H_3$ , the hole  $H_4$  covers the hole  $H_2$ , and the process becomes cyclic. In other words, after two iterates of the disk  $D$ , the map  $f|_{f^2D}$  becomes a map of a disk with *two periodic holes* that increase in size under each consequent iterate.

- (3)  $O \in fA$  [Fig. 4(c3)]. The second iterate of the map  $f$  again gives three possibilities for the mutual arrangement between  $O$  and  $fD_2$ :
  - (i) If  $O \notin fD_2$ , then  $f^2D$  is the map from Case 2, and generates an infinite number of holes.
  - (ii) If the image  $fH_2 = H_3$  covers the point  $O$ , then we obtain the map  $f|_{f^3D}$  of the disk with *three periodic holes*  $H_1, H_2, H_3$ . This number of holes remains constant under further iterates of the map, and the holes are cyclic (periodic) such that  $fH_3 = H_4 \supset H_1, fH_4 = H_5 \supset H_2, fH_5 \supset H_3, \dots$
  - (iii) If  $O \in f^2A$ , then this case is similar to the above considered possibility (3) and one can obtain a map of the disk with four holes.

Further consideration leads to the following assertion: If  $O \in H_k = f^{k-1}(H_1)$  and  $O \notin H_i, i = 1, 2, \dots, k - 1$ , then the map  $f$  is a map of the disk having  $k$  holes. As in the previous case of three holes, these holes are periodic:  $H_1 \supset H_2, H_2 \supset H_3, \dots, H_{k-1} \supset H_k, H_k \supset H_1$ . It is worth noticing that one can “insert” a period- $k$  unstable orbit in the holes  $H_i, i = 1, \dots, k$  and the holes may be thought of as the repelling domains of this orbit.

The transition between maps with  $k - 1$  and  $k$  holes is caused by a  $k$ -loop homoclinic bifurcation of the saddle  $E_\delta$ . In terms of the map  $f$ , this amounts to the situation where the point  $O$  hits the border of the hole  $H_{k-1}, \partial H_{k-1}$ , from the inside, giving rise to the hole  $H_k$ . At the bifurcation moment, the

hole  $H_k$  is joined to the hole  $H_{k-1}$ . Figure 5 gives the details for the birth of the second hole  $H_2$  via the one-loop homoclinic bifurcation.

It is worth noticing that the map  $f$  of the disk with  $k > 1$  holes belongs to a family of mappings that are not studied in the theory of dynamical systems in terms of the rotation properties of their limit sets around the holes. The only known example of attractors existing in such maps is the hyperbolic Plykin attractor [Plykin, 1974], arising in a two-dimensional map with three holes. A general construction of the vector field admitting the Plykin attractor was first presented by Belykh [2000]. Here, we will give the conditions under which an attractor homotopic to the Plykin attractor occurs in the neuron model (1). We will also discuss new homoclinic bifurcations leading to the emergence of Plykin-like attractors.

### 3.3. Plykin-like attractors and new homoclinic bifurcations

Denote  $\delta = \delta_{h_k}(\mu), k = 1, 2, \dots$ , the values of the bifurcation parameter  $\delta$  corresponding to the  $k$ -loop homoclinic bifurcation of the saddle  $E_\delta$ . These values are ordered as follows:  $\delta_{h_1}(\mu) < \delta_{h_2}(\mu) < \delta_{h_3}(\mu) < \dots < \delta_s$ . Let us consider the bifurcation transitions and the appearance of attractors with increasing  $\delta$  from  $\delta < \delta_{h_1}$ .

#### 3.3.1. One-loop homoclinic bifurcation

Let  $\delta - \delta_{h_1} < 0$  be small. This implies for the map  $f$ , that the point  $O$  lies in the hole  $H_1$  (Case 1). It follows from the bifurcation theory [Shilnikov, 1998] that there exists a saddle limit cycle passing by a small neighborhood of the saddle  $E_\delta$ . This cycle merges into the homoclinic loop for  $\delta = \delta_{h_1}$ . At this moment,  $O$  is located at the point where

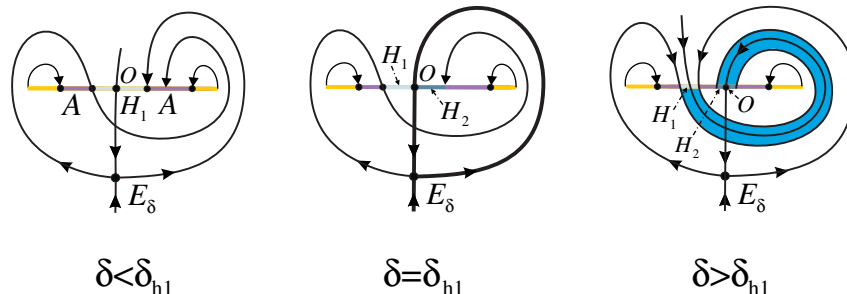


Fig. 5. Schematic pictures showing the formation of periodic holes  $H_1$  and  $H_2$ . The one-loop homoclinic bifurcation arising at  $\delta = \delta_{h_1}$  gives rise to the two holes and leads to the emergence of a Smale horseshoe (cf. Fig. 6).

two holes  $H_1$  and  $H_2 = f(H_1)$  join each other. Note that the saddle cycle had appeared through a saddle-node cycle bifurcation preceding the homoclinic bifurcation. As illustrated in Fig. 5, a further increase in  $\delta$  leads to the destruction of the homoclinic and to the separation of the holes  $H_1$  and  $H_2$ . There are two possibilities for the position of the point  $O$ .

- (a)  $O \notin H_2$ . This leads to the formation of an infinite sequence of holes  $H_3, H_4, \dots, H_\infty$ , when iterating and, according to standard bifurcation theory, does not give birth to any limiting set.
- (b) The point  $O$  falls into the hole  $H_2$  right away after the bifurcation. As discussed before, this results in the formation of two periodic holes  $H_1$  and  $H_2$  (see Fig. 5) and leads to the birth of a new limiting set. In terms of the original system (2), this situation amounts to the destruction of the homoclinic loop  $h_\mu$  [cf. Fig. 3(a)] in a way where the trajectories from a neighborhood of the nonleading manifold  $W_\mu^n$  intersect the cross-section  $D$  to the left from the leading line  $w^l$ . This bifurcation has not previously been studied, and the structure of the limiting set as well the properties of the attractor associated with a map with two holes are unknown. However, we can prove that this bifurcation at least leads to the formation of a chaotic saddle, arising far from the homoclinic loop's neighborhood. Figure 6 gives a geometrical support for the proof. Note that this bifurcation is similar in some respects to the codimension-two

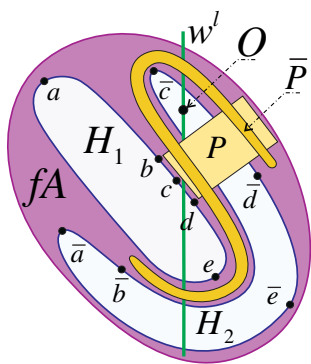


Fig. 6. Appearance of a Smale horseshoe. Two periodic holes  $H_1$  and  $H_2$  are generated through the one-loop homoclinic bifurcation. Five points  $(a, b, c, d, e)$  located on the border of  $H_1$  are mapped into five points  $(\bar{a}, \bar{b}, \bar{c}, \bar{d}, \bar{e})$  on the border of  $H_2$ , respectively. The rectangular  $P$  is mapped into the horseshoe  $\bar{P}$ .

bifurcation giving rise to the cusp horseshoe [Homburg et al., 1994].

### 3.3.2. Two-loop homoclinic bifurcation

The secondary (two-loop) homoclinic bifurcation arising at  $\delta_{h_2}$  leads to the generation of the third hole  $H_3$ . As before, there exist two equal possibilities for the position of  $O$ . The first situation when the point  $O$  does not belong to the hole  $H_3$  is not interesting and, similar to (a), it does not lead to the emergence of any attractor. The second possibility on the contrary, when  $O$  falls into the third hole  $H_3$  (see Fig. 7) and the three holes becomes periodic, is of great interest for our study. Here, the flow-defined map  $f$  becomes a map with three holes, matching the Plykin example [Plykin, 1974] of a planar hyperbolic attractor. The map  $f$  has a limit set containing horseshoes (directly from its geometrical properties) and corresponds to a strange attractor  $\Phi$  of the slow-fast system (1), obtained by the embedding of the three-hole attractor of  $f$  into the 3D phase space. The existence of the attractor  $\Phi$  is ensured by the existence of the global section and trapping zone  $G$ . Consequently, the attractor  $\Phi$  is homotopic to the Plykin attractor and has the possibility to be hyperbolic. However, the question of attractor  $\Phi$ 's hyperbolicity remains unstudied.

The topology of the attractor  $\Phi$  is complicated: Existing in the spiking-bursting transition region, it more likely corresponds to a regime of bursting

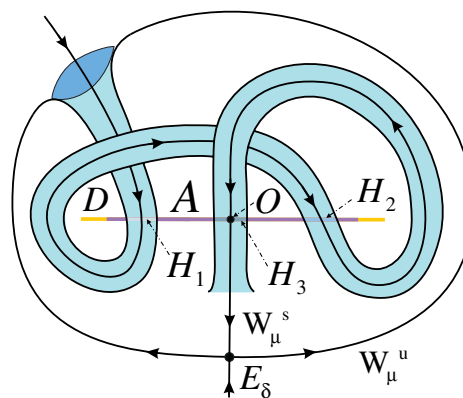


Fig. 7. Schematic sketch for the Plykin-like attractor, defined by the map with three periodic holes  $H_1, H_2$  and  $H_3$ . The point  $O$  falls into the third hole  $H_3$  after the two-loop homoclinic bifurcation (not shown in this figure). The attractor occurs in the parameter region  $\delta_{h_2} < \delta < \delta_{h_3}$  and lies in the phase space, corresponding to the region  $A \setminus \bigcup_{i=1}^3 H_i$  on the cross-section  $D$ .

where chaotic fast repetitive spiking sporadically alternates with an irregular quiescent state. It is hard (if at all possible) to say which sequence of (unstudied) bifurcations leads to the transition from tonic spiking, as existing in the region  $\delta < \delta_s$ , to this type of bursting.

Subsequent  $(k-1)$ -loop homoclinic bifurcations can lead to the formation of maps with  $k$  ( $k > 3$ ) holes. The topology and bifurcation scenarios leading to the occurrence of the corresponding Plykin-like attractors can even be more complicated than those for the three-hole attractor  $A$ . This shows that a complete description of possible bifurcation transitions between tonic spiking and bursting remains open.

#### 4. Conclusions

Introducing a global cross-section for trajectories of a generic neuron model (1), we have constructed a Poincaré return map which gives an accurate account for the dynamics, bifurcations and attractors existing in the neuron model. This map constitutes a nontrivial link between the Wang's description [Wang, 1993] of neuron dynamics in terms of the map of a disk into itself and Terman's concept [Terman, 1991, 1992] of winding numbers related to the map of the disk into an annulus.

Surprisingly, we have discovered that the Poincaré map can be a map of the disk with  $k$  periodic holes. A particular case is the map with three holes, matching the Plykin example of a planar hyperbolic attractor. Therefore, we have shown that the neuron model is expected to have a hyperbolic attractor. However, we have not performed the analysis of the discovered attractor's hyperbolic properties. The Plykin-like attractor exists in a parameter region between two- and three-loop homoclinic bifurcations of the saddle and can be found and studied numerically in concrete neuron models. The 3D Hindmarsh–Rose model satisfies all the assumptions on the system topology and is a first candidate for the existence of a Plykin-like attractor. In our study, we have restricted our attention to 3D systems having a single saddle equilibrium with a 2D unstable and 1D stable manifold. However, similar attractors may occur in 4D models having a unique saddle equilibrium point with 2D stable and 2D unstable manifolds. Possible examples include 4D Hodgkin–Huxley-type models.

We have shown that multiloop homoclinic bifurcations can lead to the emergence of strange

attractors corresponding to planar attractors of the Poincaré map with many periodic holes. The homoclinic bifurcations that we are facing do not appear to have been previously analyzed. The analysis of such bifurcation transitions remains a fundamental problem for bifurcation theory.

#### Acknowledgments

The authors are grateful to Andrey Shilnikov and Dmitry Turaev for helpful discussions. This work was supported in part by the Swiss National Science Foundation through (Grant No. 2100-065268), INTAS (Grant No. 01-2061), the EU Commission (BioSim, Grant No. 005137), RFFI (Grant No. 02-01-00968), and scientific program “Russian Universities” (Grant No. 1905).

#### References

- Belykh, V. N., Pedersen, N. F. & Soerensen, O. H. [1977] “Shunted Josephson junction model. II. The non-autonomous case,” *Phys. Rev.* **B16**, 4860–4871.
- Belykh, V. N. [2000] “A smooth dynamical system having a unique saddle equilibrium point may generate the Plykin attractor,” *Abstr. Int. Conf. Differential Equations and Dynamical Systems*, Suzdal (Steklov Math. Institute Press), pp. 13–15.
- Belykh, V. N., Belykh, I. V., Colding-Jørgensen, M. & Mosekilde, E. [2000] “Homoclinic bifurcations leading to bursting oscillations in cell models,” *Europ. Phys. J.* **E3**, 205–219.
- Gavrilov, N. S. & Shilnikov, L. P. [1972] “On three-dimensional dynamical systems close to systems with a structurally unstable homoclinic curve: I,” *Math. USSR Sbornik* **88**, 467–485.
- Golubitsky, M., Josic, K. & Kaper, T. [2001] “An unfolding theory approach to bursting in fast–slow systems,” in *Festschrift Dedicated to Floris Takens, Global Analysis of Dynamical Systems*, pp. 277–308.
- Gonchenko, S. V., Shilnikov, L. P. & Turaev, D. V. [1996] “Dynamical phenomena in systems with structurally unstable Poincaré homoclinic orbits,” *Int. J. Chaos* **6**, 1–17.
- Guckenheimer, J. & Holmes, P. [1990] *Nonlinear Oscillations, Dynamical Systems, and Bifurcations of Vector Fields*, Applied Mathematical Sciences, Vol. 42 (Springer-Verlag, NY).
- Guckenheimer, J. & Oliva, R. A. [2002] “Chaos in the Hodgkin–Huxley model,” *SIAM J. Appl. Dyn. Syst.* **1**, 105–114.
- Hindmarsh, J. L. & Rose, R. M. [1984] “A model of neuronal bursting using three coupled first order differential equations,” *Proc. Roy. Soc. London* **B221**, p. 87.

- Homburg, A., Kokubu, H. & Krupa, M. [1994] "The cusp horseshoe and its bifurcation in the unfolding of an inclination-flip homoclinic orbit," *Erg. Th. Dyn. Syst.* **14**, 667–693.
- Hunt, T. J. & Mac Kay, R. S. [2003] "Anosov parameter values for the triple linkage and a physical system with a uniformly chaotic attractor," *Nonlinearity* **16**, 1499–1510.
- Izhikevich, E. M. [2000] "Neural excitability, spiking and bursting," *Int. J. Bifurcation and Chaos* **10**, 1171–1266.
- Newhouse, S. E. [1974] "Diffeomorphisms with infinitely many sinks," *Topology* **13**, p. 918.
- Ovsyannikov, I. M. & Shilnikov, L. P. [1992] "Systems with a homoclinic curve of multi-dimensional saddle-focus type, and spiral chaos," *Math. USSR Sbornik* **73**, 415–443.
- Palis, J. & Pugh, C. [1974] *Fifty Problems in Dynamical Systems*, Lecture Notes in Mathematics, Vol. 486, pp. 34–353.
- Plykin, R. [1974] "Sources and sinks for A-diffeomorphisms," *Math. USSR Sbornik* **23**, 233–253.
- Rinzel, J. [1987] "A formal classification of bursting mechanisms in excitable systems," in *Mathematical Topics in Population Biology, Morphogenesis, and Neurosciences*, eds. Teramoto, E. & Yamaguti, M., Lecture Notes in Biomathematics, Vol. 71 (Springer-Verlag, Berlin), pp. 251–291.
- Rinzel, J. & Ermentrout, B. [1989] "Analysis of neural excitability and oscillations," in *Methods in Neuronal Modeling*, eds. Koch, C. & Segev, I. (MIT Press, Cambridge, MA), pp. 251–291.
- Shilnikov, L. P. [1984] *Bifurcation Theory and Turbulence*, Nonlinear and Turbulent Processes in Physics, Vol. 3 (Harwood Academic Publ.), pp. 1627–1635.
- Shilnikov, L. P., Shilnikov, A. L., Turaev, D. V. & Chua, L. O. [1998] *Methods of Qualitative Theory in Nonlinear Dynamics (Part I)*, World Scientific Series on Nonlinear Science, Series A, Vol. 4.
- Shilnikov, L. P., Shilnikov, A. L., Turaev, D. V. & Chua, L. O. [2001] *Methods of Qualitative Theory in Nonlinear Dynamics (Part II)*, World Scientific Series on Nonlinear Science, Series A, Vol. 5.
- Shilnikov, A. L., Shilnikov, L. P. & Turaev, D. V. [2004] "On some mathematical topics in classical synchronization. A tutorial," *Int. J. Bifurcation and Chaos* **14**, 2143–2160.
- Shilnikov, A. L., Calabrese, R. & Cymbalyuk, G. [2005] "Mechanism of bi-stability: Tonic spiking and bursting in a neuron model," *Phys. Rev.* **E71**, 056214.
- Shilnikov, A. L. & Cymbalyuk, G. [2005] "Transition between tonic-spiking and bursting in a neuron model via the blue-sky catastrophe," *Phys. Rev. Lett.* **94**, 048101.
- Terman, D. [1991] "Chaotic spikes arising from a model of bursting in excitable membranes," *SIAM J. Appl. Math.* **51**, 1418–1450.
- Terman, D. [1992] "The transition from bursting to continuous spiking in excitable membrane models," *J. Nonlin. Sci.* **2**, 133–182.
- Turaev, D. V. & Shilnikov, L. P. [1995] "On a blue sky catastrophe," *Soviet Math. Dokl.* **342**, 596–599.
- Wang, X.-J. [1993] "Genesis of bursting oscillations in the Hindmarsh–Rose model and homoclinicity to a chaotic saddle," *Physica* **D62**, 263–274.